

Slit1a Inhibits Retinal Ganglion Cell Arborization and Synaptogenesis via Robo2-Dependent and -Independent Pathways

Douglas S. Campbell,^{1,5,*} Sydney A. Stringham,¹ Adam Timm,² Tong Xiao,³ Mei-Yee Law,¹ Herwig Baier,³ Michael L. Nonet,² and Chi-Bin Chien^{1,4,*}

¹Department of Neurobiology and Anatomy, 401 MREB, University of Utah Medical Center, 20 North 1900 East, Salt Lake City, UT 84132, USA

²Department of Anatomy and Neurobiology, Washington University School of Medicine, Saint Louis, MO 63110, USA

³Department of Physiology, Program in Neuroscience, University of California, San Francisco, San Francisco, CA 94143, USA

⁴Brain Institute, University of Utah, Salt Lake City, UT 84112, USA

⁵Present address: RIKEN Brain Science Institute, 2-1 Hirosawa, Wako, Saitama, 351-0198, Japan.

*Correspondence: douglas.campbell@cantab.net (D.S.C.), chi-bin.chien@neuro.utah.edu (C.-B.C.)

DOI 10.1016/j.neuron.2007.06.034

SUMMARY

Upon arriving at their targets, developing axons cease pathfinding and begin instead to arborize and form synapses. To test whether CNS arborization and synaptogenesis are controlled by Slit-Robo signaling, we followed single retinal ganglion cell (RGC) arbors over time. *ast* (*robo2*) mutant and *slit1a* morphant arbors had more branch tips and greater arbor area and complexity compared to wild-type and concomitantly more presumptive presynaptic sites labeled with YFP-Rab3. Increased arborization in *ast* was phenocopied by dominant-negative Robo2 expressed in single RGCs and rescued by full-length Robo2, indicating that Robo2 acts cell-autonomously. Time-lapse imaging revealed that *ast* and *slit1a* morphant arbors stabilized earlier than wild-type, suggesting a role for Slit-Robo signaling in preventing arbor maturation. Genetic analysis showed that Slit1a acts both through Robo2 and Robo2-independent mechanisms. Unlike previous PNS studies showing that Slits promote branching, our results show that Slits inhibit arborization and synaptogenesis in the CNS.

INTRODUCTION

The correct formation of synaptic connections is critical for the functioning of the nervous system. During development, growth cones navigate to their targets by using a series of cues along their pathway. Upon reaching their targets, their morphology changes dramatically with the formation of branches and synapses. Recent in vivo imaging studies have begun to elucidate the dynamics and mechanisms involved in the processes of arborization

and synaptogenesis in the CNS (Alsina et al., 2001; Cohen-Cory and Fraser, 1995; Meyer and Smith, 2006; Niell et al., 2004). However, we know only a few of the signals that control these processes in vivo (Jin, 2002; Yeo et al., 2004). The zebrafish retinotectal system is uniquely suited for the study of arborization and synaptogenesis, as the embryos are easily manipulated genetically, develop externally, and are transparent, enabling in vivo imaging (Hutson et al., 2004). Here, we combine genetics and in vivo imaging in zebrafish to show that Slit-Robo signaling, in addition to its known role in retinal axon guidance (Fricke et al., 2001; Hutson and Chien, 2002; Plump et al., 2002), also plays a later role in mediating retinal ganglion cell arborization and synaptogenesis in vivo.

Growing RGC axons navigate through the brain to reach the optic tectum in the dorsal midbrain. In the zebrafish, RGC growth cones begin to form arbors as soon as they have reached the topographically correct region of the tectum (Stuermer, 1988). Arborization and synaptogenesis begin and visual responses can be elicited by 3 days postfertilization (dpf) (Easter and Nicola, 1996). At this age, RGC axonal arbors and tectal dendrites are highly dynamic, both adding and retracting branch tips (Meyer and Smith, 2006; Niell et al., 2004; Stuermer, 1988). To ensure correct neural connectivity, the processes of arborization and synaptogenesis must be highly regulated and coordinated, to precisely arrange pre- and postsynaptic components to form a functional synapse (Waites et al., 2005). Recently, synapse formation in RGC arbors has been demonstrated to occur concurrently with arborization (Meyer and Smith, 2006). Arbor growth can be regulated by several factors, including synaptic activity and extracellular cues, notably neurotrophins (Alsina et al., 2001; Cohen-Cory and Fraser, 1995), which may interact with common cytoskeletal regulators to affect arborization. However, in contrast to the panoply of known axon guidance ligands, few ligands are known to control axon branching.

Members of the Roundabout (Robo) and Slit gene families were first identified in invertebrates as repulsive

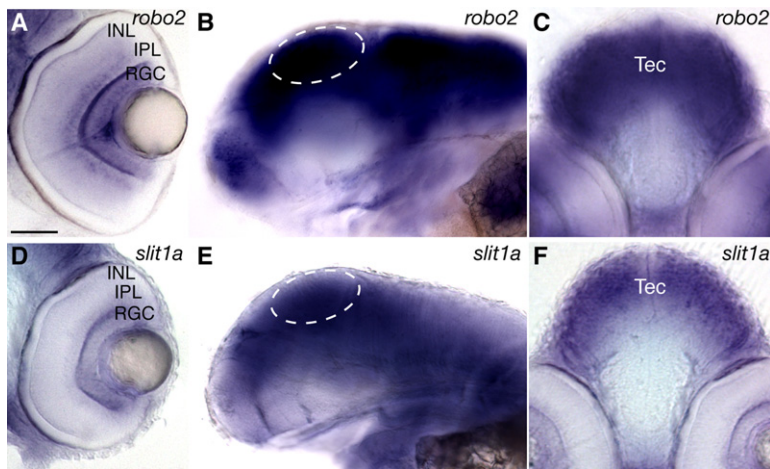


Figure 1. Zebrafish *slit1a* and *robo2* Are Expressed in the Eye and Optic Tectum during RGC Arborization and Synaptogenesis

Shown are whole-mount lateral views ([B and E]; anterior left, dorsal up), and transverse vibratome sections through the retina ([A and D]; dorsal up) and optic tectum ([C and F]; dorsal up) at 76 hpf. *robo2* is highly expressed throughout the tectum and RGCs (A–C). *slit1a* is strongly expressed throughout the tectum and weakly in RGCs (D–F). RGC, retinal ganglion cells; IPL, inner plexiform layer; INL, inner nuclear layer. Dashed ovals indicate the tectum. Scale bar, 50 μ m.

receptors and ligands, respectively (Kidd et al., 1999; Wong et al., 2002). In vertebrates, Slit proteins have been shown to bind Robo receptors (Brose et al., 1999; Li et al., 1999) and to repel, for example, spinal, olfactory, and retinal axons (Wong et al., 2002). Additionally, Slit proteins induce branching of mammalian sensory neurones in vitro (Wang et al., 1999), and overexpression of Slit2 in zebrafish embryos induces branching of trigeminal sensory axons in a Robo2-dependent manner in vivo (Yeo et al., 2004). It has not previously been tested whether Slit-Robo signaling also regulates arborization in the CNS. Furthermore, very little is known about potential roles for Slit-Robo signaling in synaptogenesis.

In the developing zebrafish retinotectal system, *robo2* is expressed in RGCs as they navigate toward their main target, the optic tectum (Fricke et al., 2001; Lee et al., 2001). Our laboratory has previously shown that *robo2* is the gene defective in the *astray* (*ast*) mutant and is required eye-autonomously for RGC axon pathfinding (Fricke et al., 2001). Slits surrounding the optic chiasm appear to signal through Robo2 to prevent and correct pathfinding errors, shaping the chiasm by surround repulsion (Hutson and Chien, 2002; Plump et al., 2002). Given the branch-promoting functions previously shown for Slit2 and the requirement for Robo2 during retinal axon pathfinding, we wondered whether Slit-Robo signaling might also play a role in retinotectal arborization and synaptogenesis. We found that of the zebrafish *slit* and *robo* genes, only *robo2* and *slit1a* are expressed in the RGCs and tectum during arborization. Removal of *robo2* or *slit1a* function resulted in increased numbers of branch tips, arbor area, and arbor complexity, showing that Slit-Robo signaling inhibits arborization in vivo in the vertebrate CNS. Furthermore, we find a role for Slit-Robo signaling in inhibiting synaptogenesis. Manipulation of Robo2 function in individual RGCs shows that it acts cell-autonomously to inhibit arborization. Genetic interaction experiments show that *slit1a* inhibits arborization via both *robo2*-dependent and *robo2*-independent pathways. We also find that extra branching in *ast* arbors arises early dur-

ing arborization and is followed by a decrease in branch tip dynamics, consistent with a role for Slit-Robo signaling in preventing the premature maturation of RGC arbors.

RESULTS

slit1a and *robo2* Are Expressed in the Tectum and RGCs, Consistent with Roles in Arborization and Synaptogenesis

To determine which members of the Robo and Slit protein families could be involved in regulating arborization and synaptogenesis, we performed in situ hybridization at 76 hr postfertilization (hpf) for the four *robo* genes and four *slit* genes of zebrafish. *robo2* was strongly expressed in the RGC layer of the retina and throughout the tectum (Figures 1A–1C). In contrast, the other three *robo* genes were not expressed in the RGCs or tectum, except for a few tectal cells that expressed *robo3* (see Figure S1 in the Supplemental Data available with this article online). *slit1a* was expressed throughout the tectum and weakly in RGCs (Figures 1D–1F). The other three *slit* genes were not expressed in the tectum, nor in the RGC layer of the retina (Figure S1). Thus, of the *robo* and *slit* genes, only *robo2* and *slit1a* are expressed appropriately to mediate RGC arborization or synaptogenesis.

robo2 and *slit1a* Inhibit RGC Arborization in the Tectum In Vivo

We next tested whether *robo2* and *slit1a* are required for retinotectal arborization in the tectum, by analyzing individual arbors in *ast* (*robo2*) mutants and in embryos injected with antisense morpholino oligonucleotides directed against *slit1a* (*slit1a* morphants).

To label individual RGC axons, we transiently expressed a membrane-targeted form of green fluorescent protein (GAP43-GFP or mGFP) under the control of the *bm3c* (also known as *brn3.1* or *pou4f3*) enhancer, which drives expression in a subpopulation of ~50% of RGCs (Xiao et al., 2005). Plasmid injection into one to four cell embryos resulted in mGFP expression in one or a few

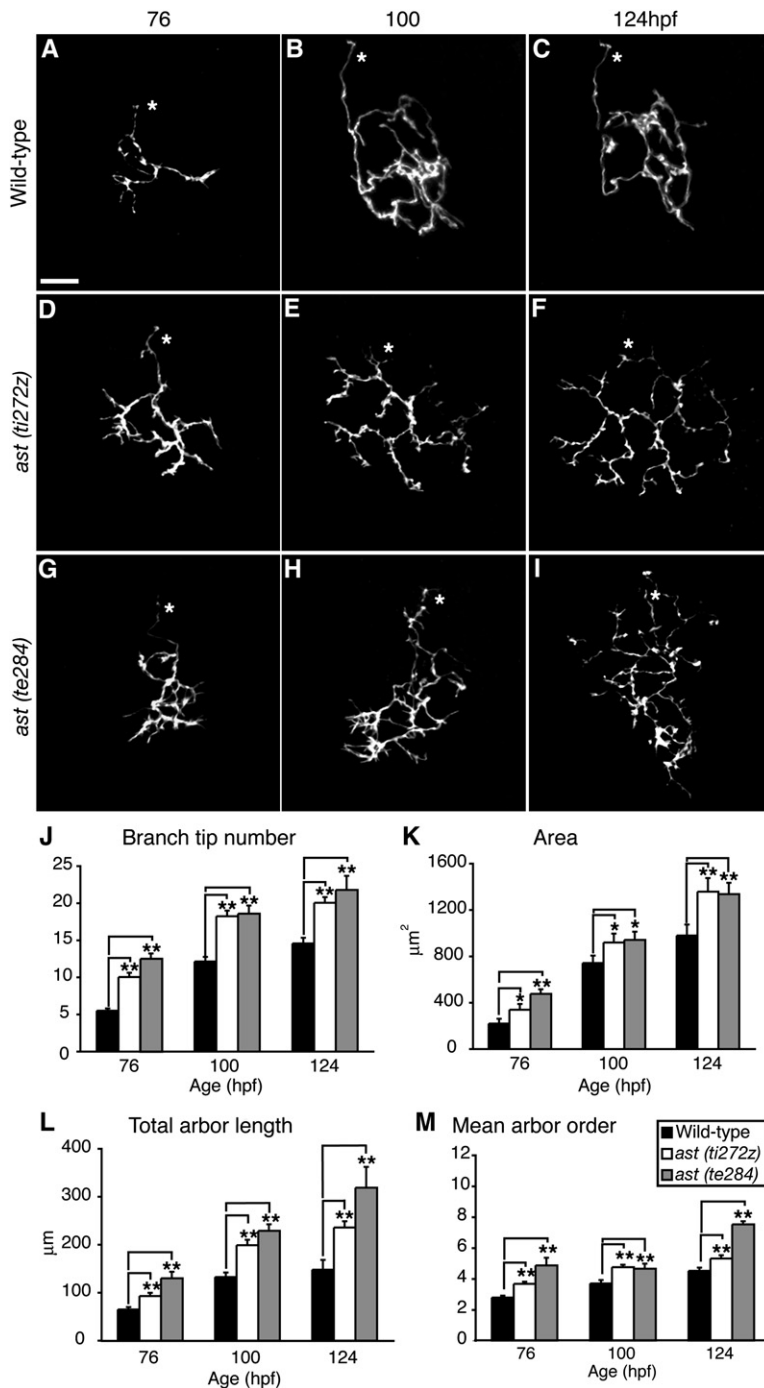


Figure 2. Lack of Robo2 Function in *astray* Mutant Embryos Results in Increased Size and Complexity of RGC Arbors

Repeated imaging of WT RGC arbors expressing mGFP under the control of the *brn3c* promoter reveals that they develop in a stereotypical manner. The numbers of branch tips, arbor area, total arbor length, and arbor order increase from 76 to 124 hpf ([A–C], quantified in [J–M]). RGC arbors from two *ast* mutant alleles (*ti272z* and *te284*) possess significantly increased numbers of branch tips, arbor area, total arbor length, and mean arbor order compared to age-matched WT embryos ([D–F] and [G–I], quantified in [J–M]). Confocal projections in (A)–(I) are dorsal views, anterior up. White * indicates the parent axon. ≥ 19 arbors from ≥ 19 embryos analyzed per genotype. Error bars represent SEM. * $p < 0.05$, ** $p < 0.01$. Scale bar, 10 μm .

RGC axons and their arbors in $\sim 10\%$ of injected embryos by 76 hpf (Hutson et al., 2004), the stage at which visual responses begin to be elicited in the zebrafish (Easter and Nicola, 1996). This allowed us to examine the morphology of single developing caudomedial arbors by repeated imaging (Figures 2A–2I). Wild-type (WT) embryos underwent a stereotypical increase in branch tip number, total arbor area, total arbor length, and arbor order during the period 76–124 hpf (Figures 2A–2C; quantified in Fig-

ures 2J–2M; quantification described in Figure S2). These increases are consistent with previous studies in the zebrafish retinotectal system (Schmidt et al., 2000; Tokuoka et al., 2002).

Slit proteins can promote sensory axon branching in PNS neurones in vitro (Wang et al., 1999) and in vivo (Yeo et al., 2004). To test whether Slit-Robo signaling plays a role in the developing vertebrate CNS, we imaged RGC arbor development between 76 and 124 hpf in two

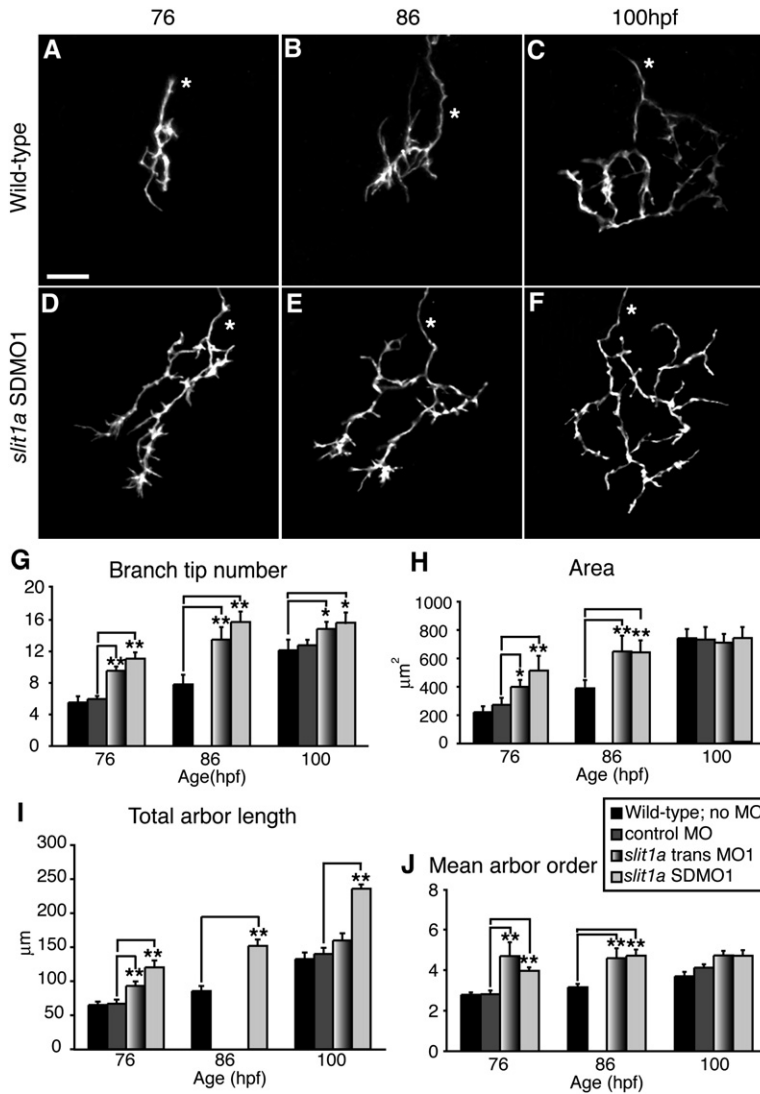


Figure 3. Knockdown of Slit1a Function Leads to Increased Size and Complexity of RGC Arbors

Knockdown of Slit1a protein with either translation- (*slit1a* trans MO1) or splice-blocking morpholinos (*slit1a* SDMO1) leads to a significant increase in the number of branch tips, total arbor length, arbor area, and mean arbor order (D–J) compared to control morphant (*control* MO) and WT RGC arbors (*no* MO) (A–C and G–J). Confocal images in (A)–(F) show repeated imaging of single arbors, labeled with *bm3c:GAL4, UAS:mGFP*. Dorsal views, anterior up. White * indicates the parent axon. ≥ 19 arbors from ≥ 19 embryos analyzed per condition. Error bars represent SEM. * $p < 0.05$, ** $p < 0.01$. Scale bar, 10 μm .

mutant alleles of *ast* (*robo2*): *ti272z*, which encodes a premature stop codon in the extracellular domain and is presumably a null mutation; and *te284*, which encodes a missense mutation in the transmembrane domain and is hypomorphic (Fricke et al., 2001; Karlstrom et al., 1996). Despite the RGC pathfinding errors in *ast* embryos, many axons still reach the tectum. When comparing either *ast* allele to WT controls at 76 hpf, we observed no obvious differences in axon outgrowth or entry into the tectum (data not shown). When we analyzed RGC arbors on the tectum between 76 and 124 hpf, however, we found that arbors in both alleles of *ast* bore approximately twice as many branch tips as WT arbors and had increased total arbor lengths, arbor areas, and mean arbor order (Figures 2D–2I; quantified in Figures 2J–2M).

Next, we used antisense morpholino oligonucleotides (MOs) to partially knock down Slit1a function, restricting ourselves to low doses to avoid potentially nonspecific effects (Experimental Procedures). MOs have previously

been used to knock down Slit1a (Barresi et al., 2005), and we observe “*ast*-like” pathfinding errors in the optic tract with the *slit1a* MOs used here (L.D. Hutson, M.E. Hardy, D.S.C., and C.-B.C., unpublished data). We found that injection of either *slit1a* translation- or splice-blocking MOs, but not control MO, led to an arborization phenotype at 76 and 86 hpf similar to *ast* mutants (Figures 3A, 3B, 3D, and 3E; quantified in Figures 3G–3J). Morphant phenotypes were weaker at 100 hpf, probably due to a decrease over time in MO effectiveness (Figures 3C and 3F; quantified in Figures 3G–3J). These results show that, in contrast to the branch promotion seen in previous PNS studies (Wang et al., 1999; Yeo et al., 2004), Slit-Robo signaling inhibits arborization in zebrafish RGCs.

Robo2 Acts Cell-Autonomously in RGC Arbors to Inhibit Arborization

Since Robo2 is required eye-autonomously for RGC axon pathfinding (Fricke et al., 2001), we hypothesized that

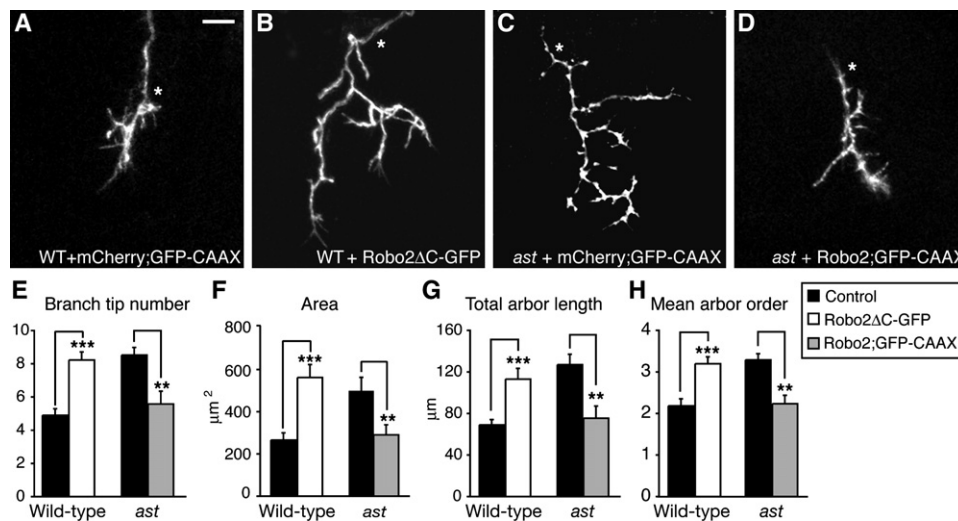


Figure 4. Robo2 Acts Cell-Autonomously in RGCs to Inhibit Arborization

Confocal micrographs of GFP labeling in 76 hpf WT and *ast* RGC arbors expressing *UAS:mCherry-IRES:EGFP-CAAX* (mCherry;GFP-CAAX), dominant-negative Robo2 tagged with GFP (Robo2ΔC-GFP) or full-length Robo2 (Robo2; GFP-CAAX), driven by coinjection of *isl3:GAL4* (A–D). Expression of Robo2ΔC-GFP in RGCs leads to an increase in branch tip number, arbor area, total arbor length, and arbor order similar to that found in *ast* mutant arbors (A versus B); quantified in (E)–(H). Expression of Robo2; GFP-CAAX in RGCs rescues the *ast* phenotype (C versus D); quantified in (E)–(H). Dorsal views, anterior up. White * indicates the parent axon. ≥ 14 arbors from ≥ 14 embryos analyzed per condition. Error bars represent SEM. ** $p < 0.01$, *** $p \leq 0.0001$. Scale bar, 10 μm .

Robo2 function is required in RGC arbors to mediate its inhibitory effect on arborization. The alternate hypothesis, that increased arborization is indirectly caused by changes in the brain, was made less likely by several observations. In *ast* or *slit1a* morphants, axons that arborized on the tectum reached it via normal trajectories (Figure S3), and so likely encountered a normal environment en route. General brain and eye patterning appeared normal (Figure S4), and *ast* homozygotes are homozygous viable and form a normal forebrain axon scaffold (Fricke et al., 2001), further arguing against gross changes in brain patterning. Finally, changes in arborization cannot easily be attributed to changes in retinotectal topography, which is normal in *ast* mutants (Lee et al., 2004).

However, since during arborization *robo2* is expressed not only in RGCs but also in the tectum (Figures 1A–1C), it was conceivable that Robo2 signaling could act in tectal dendrites, thence acting back on RGC arbors. Therefore, we tested directly whether Robo2 acts in individual RGC axons, using DNA injection to either phenocopy or rescue the *ast* phenotype (Figure 4), driving expression using the *isl3* promoter, which expresses in all or nearly all RGCs (A.J. Pittman and C.-B.C., unpublished data). For phenocopy experiments, we coinjected one- to four-cell WT embryos with DNA for *isl3:GAL4* together with a cytoplasmically truncated Robo2 construct comprising the extracellular and transmembrane domains with a GFP tag (*UAS:Robo2ΔC-GFP*) (Experimental Procedures), using an mCherry;EGFP-CAAX construct (*UAS:mCherry-IRES-EGFP-CAAX*) as a control. A similar Robo2ΔC construct has previously been used to inhibit Robo signaling (Stein and Tessier-Lavigne, 2001; Yeo et al., 2004). Expression

of Robo2ΔC-GFP in WT RGCs led to more branch tips and increased arbor area, total length, and arbor order compared to controls at 76 hpf (Figures 4A and 4B; quantified in Figures 4E–4H), and indeed Robo2ΔC-expressing WT arbors were very similar to *ast* arbors (Figures 4B and 4C; quantified in Figures 4E–4H). For rescue experiments, we coinjected *ast* homozygotes with *isl3:GAL4* and a full-length Robo2;EGFP-CAAX construct (*UAS:Robo2-IRES-EGFP-CAAX*), again using mCherry;EGFP-CAAX as a control. Bicistronic constructs (Experimental Procedures) using the EMCV internal ribosome entry sequence (IRES) allowed us to visualize single Robo2-expressing arbors using membrane-localized EGFP (Figures 4C and 4D); dual-color imaging of mCherry;EGFP-CAAX arbors showed both mCherry and EGFP fluorescence (data not shown). *ast* arbors expressing full-length Robo2 were significantly less complex than *ast* controls for all four arbor parameters and indeed resembled WT arbors expressing mCherry;EGFP-CAAX (Figures 4C and 4D; quantified in Figures 4E–4H). These results show that Robo2 is both necessary and sufficient in RGCs, acting cell-autonomously to inhibit arborization.

Rab3 Labels Presumptive Presynaptic Sites In Vivo

To monitor synapse development in RGC arbors, we cloned the zebrafish homolog of Rab3, a GTPase associated with synaptic vesicles (Sudhof, 2004), fused YFP in-frame at its N terminus, and placed 14X UAS repeats upstream to allow transcriptional activation by GAL4 (Köster and Fraser, 2001). We confirmed that YFP-Rab3 labels presynaptic sites in vivo by expressing it in spinal motor neurones under control of the α -*tubulin* or *hb9*

promoters. We then compared the locations of YFP-Rab3-positive presynaptic puncta to neuromuscular postsynaptic elements labeled with Alexa-594-conjugated α -bungarotoxin (Figure S5). Nearly all YFP-Rab3-positive puncta (90% at 3 dpf, $n = 121$; 91% at 5 dpf, $n = 151$) overlapped with α -bungarotoxin-labeled postsynaptic ACh receptors.

When we labeled single RGC arbors by coinjecting *bm3c:GAL4VP16* and UAS:YFP-Rab3, we also found punctate YFP-Rab3 labeling (compare Figure 5B to the uniform mGFP labeling in Figure 5A). The numbers and area of YFP-Rab3 puncta were quantified by thresholding (Figures 5C and 5D; Experimental Procedures). The mean size of YFP-Rab3 puncta in RGC arbors at 76 hpf was very similar to that described for synaptophysin-GFP, another presynaptic marker (data not shown; Meyer and Smith, 2006). We conclude that YFP-Rab3 can indeed be used as a marker of presumptive presynaptic sites in zebrafish spinal and RGC neurones.

Robo2 and Slit1a Are Negative Regulators of Synaptogenesis

Previous studies have shown that the processes of arborization and synaptogenesis at the NMJ (Javaherian and Cline, 2005) and in the CNS (Alsina et al., 2001; Meyer and Smith, 2006; Ruthazer et al., 2006) are intimately connected and occur concurrently. Therefore, we hypothesized that *robo2* and *slit1a*, in addition to inhibiting branching, might also be negative regulators of RGC synaptogenesis. To test this hypothesis, we repeatedly imaged single YFP-Rab3-labeled RGC arbors from 76 to 100 hpf. YFP-Rab3 was punctate in WT RGC arbors by 76 hpf, and the number and total punctal area per arbor increased between 76 and 100 hpf (Figures 5E–5G; quantified in Figures 5K and 5L). Expression of YFP-Rab3 in *ast* arbors revealed an approximate doubling in the number and total area of puncta in *ast* compared to WT throughout this period (Figures 5H–5J; quantified in Figures 5K and 5L). Puncta density (number of puncta/total arbor length) was relatively constant in both WT and *ast*, except at 100 hpf, where puncta density was significantly decreased in *ast* compared to WT (Figure 5M). *slit1a* morphant arbors also showed increased number and total area of puncta compared to WT at 76 hpf (Figures 5N–5S; quantified in Figures 5T and 5U). However, the increase was transient, so that at 86 and 100 hpf morphant arbors appeared similar to WT (Figures 5N–5S; quantified in Figures 5T and 5U). Puncta density was unaffected in *slit1a* morphant arbors compared to WT (Figure 5V). These observations suggest that, in addition to inhibiting arborization, *robo2* and *slit1a* are also inhibitors of synaptogenesis in vivo.

Slit1a Inhibits Arborization via Robo2-Dependent and Robo2-Independent Pathways

Slit and Robo proteins are known to bind each other directly and exert their biological effects by acting as ligand-receptor pairs (Wong et al., 2002). In our system,

the expression of *slit1a* and *robo2* in the tectum and RGCs, together with the similar arborization phenotypes of *slit1a* morphants and *ast* mutants, strongly support the model that Slit1a acts through Robo2. As a further test of this model, we looked for dosage-sensitive interactions between *slit1a* and *robo2*. We observed mGFP-labeled arbors at 76 hpf in WT, *ast^{ti272z}/+* heterozygote, and *ast^{ti272z}* homozygote embryos injected with no MO, with control MO, or with *slit1a* trans MO1, again at a dose that causes partial knockdown of *slit1a* function (Figure 6). Removing one copy of *robo2* revealed no haploinsufficient arborization phenotype: *ast/+* heterozygotes were indistinguishable from WT (*ast/+* or *ast/+;control MO* compared to WT or WT;*control MO*; see Figures 6A, 6B, 6D, and 6E) by all of our quantitative measures (Figures 6J–6M). However, removing one copy of *robo2* in *slit1a* morphants caused significant increases in branch tip number, arbor area, and total arbor length (*ast/+;slit1a MO* compared to WT;*slit1a MO*; see Figure 6A, 6B, 6D, 6E, 6G, and 6H, quantified in Figures 6J–6M). Thus, combining partial loss of function of *slit1a* and of *robo2* yields supra-additive effects, implying a close genetic interaction between these two genes, as would be predicted if Slit1a signals through Robo2.

To our surprise, we noticed that arbors in *ast/+;slit1a MO* embryos were *more* complex than in *ast^{ti272z}* homozygotes, which lack all Robo2 receptor function because the *ti272z* allele encodes a stop codon in the Robo2 extracellular domain. This suggested that Slit1a has some function that does not require Robo2. To test this stringently, we analyzed the effect of knocking down *slit1a* in *ast* homozygote embryos. We found significant increases in branch tip number, arbor area, total arbor length, and mean branch order (*ast;slit1a MO* compared to *ast* or *ast;control MO*; see Figures 6C, 6F, and 6I, quantified in Figures 6J–6M). Furthermore, we observed significant increases in the number and density of YFP-Rab3 puncta between *ast* and *ast;slit1a MO* arbors (Figures 6N and 6O). Thus, in the absence of all Robo2 function, reducing Slit1a function leads to a further increase in arbor complexity and presynaptic sites. Taken together, these genetic results support the model that Slit1a signals partly through Robo2 but also show that part of Slit1a function is Robo2 independent.

ast and *slit1a* Morphant Arbor Dynamics Mature Faster Than Wild-Type

Arborization of RGCs is a highly dynamic process involving extensive rearrangement of arbors via branch tip additions and retractions (Alsina et al., 2001; Meyer and Smith, 2006). We next asked whether the *ast* and *slit1a* morphant arborization phenotypes, particularly the increase in branch tip numbers, might arise due to altered branch dynamics, i.e., rates of branch tip additions and retractions, or changes in branch tip lifetimes. To analyze branch dynamics, we performed high-resolution time-lapse imaging of mGFP-labeled RGC arbors using confocal or two-photon microscopy. We imaged arbors every 15 min

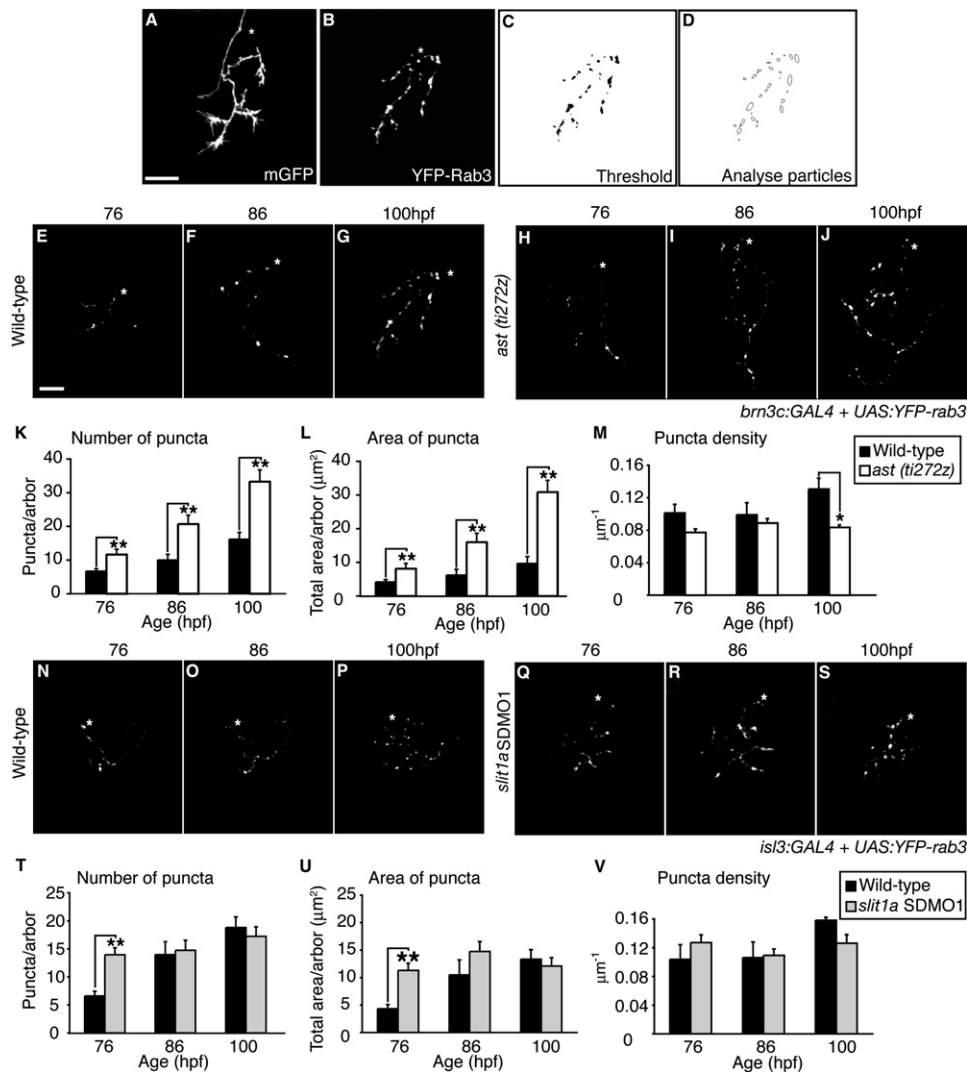


Figure 5. Robo2 and Slit1a Inhibit RGC Synaptogenesis

A confocal image of a 100 hpf RGC arbor expressing mGFP. Note the uniform expression of GFP along the entire arbor and the fine details of the filopodia-like processes (A). A confocal image of an RGC arbor of the same age expressing YFP-Rab3. Note the punctate labeling throughout the arbor and the unlabeled parent axon (B). Analysis of YFP-Rab3 puncta number and area in RGCs were performed by thresholding the confocal image and using the “analyse particle” function in ImageJ (C and D). Confocal images of the development of YFP-Rab3 expression in RGC arbors under control of the *brn3c* enhancer (E–G) and the *is3* promoter (N–S). In WT, the YFP-Rab3 expression is punctate at 76 hpf, and the mean number and total area of YFP-Rab3 puncta increase from 76 to 100 hpf (E–G, K, L, N–P, T, and U). The mean number and total area of YFP-Rab3 puncta per arbor are significantly increased in *ast (ti272z)* mutant arbors between 76 and 100 hpf compared to age-matched WT arbors (H–L). YFP-Rab3 puncta density only increases at 100 hpf in WT (M). The mean number and total area of YFP-Rab3 puncta per arbor are increased in *slit1a* morphants (*slit1a* SDMO1) compared to WT at 76 hpf but not at 86 or 100 hpf (Q–U). YFP-Rab3 puncta density/μm is not significantly different between WT and age-matched morphant arbors (V). Dorsal views, anterior up (E–J and N–S). White * indicates the parent axon. ≥ 18 arbors from ≥ 18 embryos analyzed per condition. Error bars represent SEM. ** $p < 0.01$. Scale bar, 10 μm.

during three 5 hr windows: 68–73, 80–85, and 100–105 hpf. In agreement with a previous study (Stuermer, 1988), we found that WT RGC arbors underwent two phases of arborization. An early phase (68–85 hpf) with high rates of branch tip addition and retraction was followed by a later phase (100–105 hpf), characterized by lower rates of branch tip additions and retractions (Figures 7G and 7J; Movies S1, S3, and S6). From 68–73 hpf, WT

and *ast* arbors had similar levels of branch tip additions and retractions (Figures 7G and 7J; Movies S1 and S2). However, during the second and third imaging periods, *ast* and *slit1a* morphant arbors had approximately half the number of additions and retractions as WT (Figures 7A–7F and 7J; Movies S3–S5). In fact, the addition and retraction rates for *ast* and *slit1a* morphant arbors at 80–85 hpf were very similar to those of WT arbors during

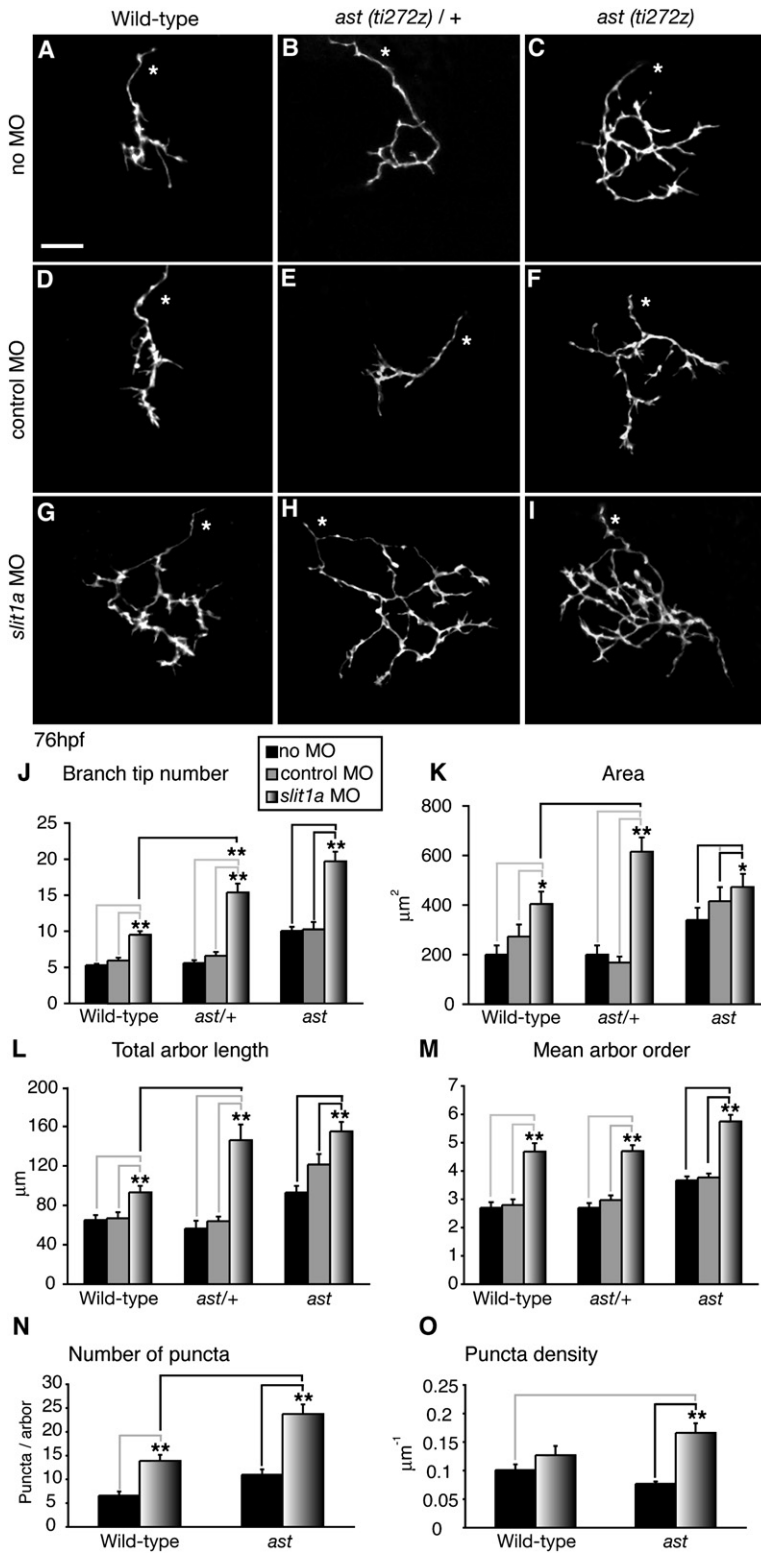


Figure 6. Slit1a Inhibits Arborization via Robo2-Dependent and Robo2-Independent Pathways

Confocal images of 76 hpf RGC arbors, labeled with *brn3c:GAL4, UAS:mGFP*, from WT, *astray (ti272z)/+* heterozygous, and *ast (ti272z)* homozygous embryos, either without MO (*no MO*) (A–C), coinjected with control MO (*control MO*) (D–F), or coinjected with control MO (*slit1a MO*) (G–I). In all three genotypes, control MO has no effect on branch tip number (J), arbor area (K), total arbor length (L), and arbor order (M). Injection of *slit1a MO* into WT embryos (WT; *slit1a MO*), partially knocking down *slit1a* function, increases arborization compared to WT or control morphants (G versus A; D, and J–M). Injection of *slit1a* trans MO into *ast/+* (*ast/+; slit1a MO*) embryos results in a further significant increase in arborization compared to WT; *slit1a MO* (H versus G); (J–M). Furthermore, arborization in *ast/+; slit1a MO* is increased compared to *ast; no MO* or *ast; control MO* (compare [H] to [F] and [C]; [J–M]). *ast; slit1a MO* embryos have significantly increased arborization compared to *ast; control MO* (I versus C and F; J–M). YFP-Rab3 puncta/arbor but not puncta density are significantly increased in *ast; slit1a MO* compared to *ast* and *slit1a MO* (N and O). Dorsal views, anterior up (A–I); white * indicates the parent axon. ≥ 19 arbors from ≥ 19 embryos analyzed per condition. Error bars represent SEM; * $p < 0.05$, ** $p < 0.01$. Scale bar, 10 μm .

100–105 hpf (Figures 7G and 7J; Movies S4–S6). Decreased branch tip addition and retraction rates in *ast* and *slit1a* morphant arbors were accompanied by an in-

crease in total branch tip lifetimes and in the proportion of stable branch tips (those that persisted for the entire 5 hr imaging session) (Figures 7A–7F, 7H, 7I, 7K, and 7L;

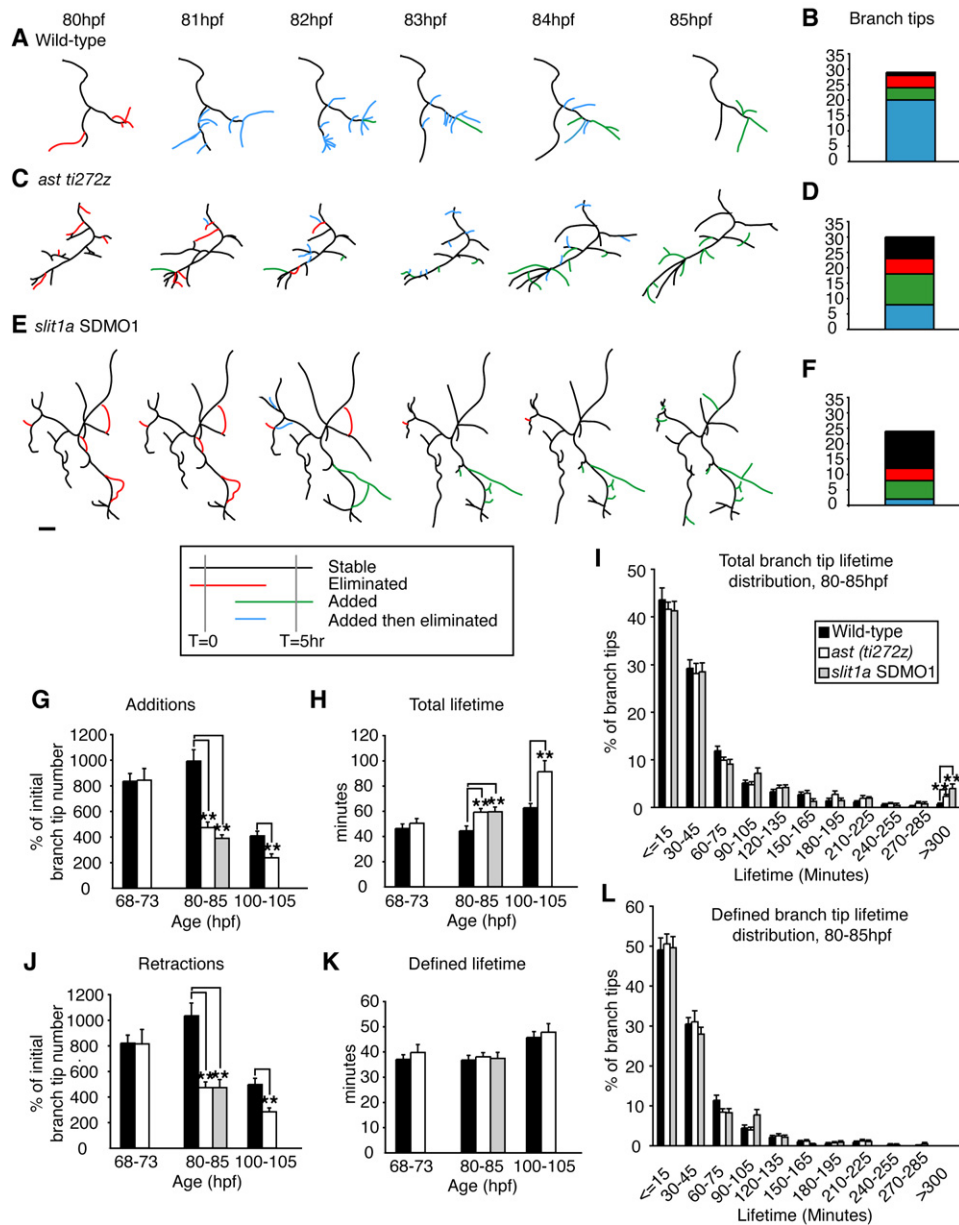


Figure 7. *ast* Mutant and *slit1a* Morphant Arbor Dynamics Mature Faster Than Wild-Type Arbors

Tracings of representative WT (A), *ast ti272z* mutant (C), and *slit1a* SDMO1 morphant (E) RGC arbors, labeled with *brn3c:GAL4, UAS:mGFP*, every hour during time-lapse imaging from 80 to 85 hpf; dorsal views, anterior up. *black*, stable branch tips; *red*, eliminated tips; *green*, added tips; *blue*, tips that were added then eliminated during imaging. The proportion of branch tips in each category is shown in (B), (D), and (F). Quantitation of dynamics in eight to ten arbors from eight to ten embryos per condition are shown in (G)–(L). Additions and retractions are shown as a percentage of initial branch tip number (G and J). All four categories were included to calculate “total” lifetimes (H and I), while only tips that were added and then eliminated were included to calculate “defined” lifetimes (K and L). Between the ages of 68 and 105 hpf, WT RGC arbors undergo two phases of arbor dynamics, with high levels of branch tip additions and retractions between 68 and 85 hpf followed by a slower phase of branch tip additions and retractions (G and J). At 80–85 hpf and 100–105 hpf, *ast* mutant and *slit1a* morphant arbors have significantly lower percentages of branch tip additions and retractions compared to WT (A–G and J). At 80–85 hpf and 100–105 hpf, *ast* mutant and *slit1a* morphant arbors also have significantly increased total but not defined branch tip lifetimes (H and K). Furthermore, during 80–85 hpf, *ast* mutant and *slit1a* morphant arbors have a significantly increased proportion of branch tips that persist throughout the imaging period ((B, D, F, and I), bars at >300 min). Error bars represent SEM. ***p* < 0.01. Scale bar, 10 μ m.

Movies S1–S7. In a few YFP-Rab3 time-lapse experiments, we observed a similar decrease in gain and loss of presynaptic puncta and increased puncta lifetimes in

ast compared to WT arbors between 80 and 85 hpf (Figure S6; Movies S8 and S9). Thus, the dynamics of branch tip addition and retraction in *ast* and *slit1a*

morphant arbors appear to mature faster than in WT, resulting in more stable arbors.

The *ast* Phenotype Arises Early during the Process of Arborization

Time-lapse imaging revealed differences between WT and *ast* and *slit1a* morphant arbors during the 80–85 hpf and 100–105 hpf imaging periods, when *ast* and *slit1a* morphant arbors are already more complex than WT arbors. This begs the question of how the phenotype initially arises. Although we did not observe a gross difference in branch tip additions and retractions between WT and *ast* at 68–73 hpf, only a small imbalance of additions over retractions would be necessary to cause an increase from four to eight branch tips per arbor. Therefore, we calculated the increase in number during each of the three 5 hr imaging periods (Figures 8A–8L; quantified in Figure 8M). *ast* arbors nearly doubled their number of branch tips from 68–73 hpf, but then showed relatively little change at 80–85 and 100–105 hpf (Figures 8A–8L; quantified in Figure 8M). In contrast, WT arbors increased in branch tip number compared to *ast* during the 80–85 hpf imaging period (Figures 8E–8H; quantified in Figure 8M). Thus, the increased numbers of branch tips in *ast* arbors arise early during arborization.

DISCUSSION

We have used a combination of genetics and in vivo imaging in the zebrafish retinotectal system to investigate the role of Slit-Robo signaling in mediating arborization and synaptogenesis, processes that are only starting to be studied in the vertebrate CNS. Global loss-of-function experiments show that *robo2* and *slit1a* are inhibitors of arborization and synaptogenesis, while local perturbation of Robo2 function in individual RGCs identifies a cell-autonomous role for Robo2 in inhibiting arborization. A strong genetic interaction between *slit1a* and *robo2* supports the model that Slit1a's effect is at least partly mediated by Robo2. However, epistasis experiments in which *ast;slit1a* MO arbors were more complex than *ast* arbors indicate that Slit1a also acts through a Robo2-independent pathway, presumably using a second receptor. Furthermore, we found that branch dynamics are altered in *ast* and *slit1a* morphant arbors, consistent with the hypothesis that Slit-Robo signaling prevents the premature maturation of RGC arbors in the optic tectum.

Our work defines an *inhibitory* role on arborization for Slit-Robo signaling. Previous studies have shown that Slit2 acts as a branch-promoting factor for mammalian sensory axons (Wang et al., 1999) and zebrafish trigeminal sensory axons (Miyashita et al., 2004; Yeo et al., 2004). During axon guidance, vertebrate Slit1 and Slit2 are known to act as repulsive cues (Wong et al., 2002). Here, we show that Slit1a negatively regulates arborization. Why do Slits encourage branching in some cases and inhibit it in others? One possibility is that this reflects the cell type being studied. Indeed, semaphorin 3A

(Sema3A) promotes branch formation of *Xenopus* retinal growth cones (Campbell et al., 2001) and inhibits branch formation in mammalian spinal neurones (Bagnard et al., 1998). Differences in neurones' responsiveness could be due to inherent differences in the level of cyclic nucleotides present, since manipulation of cyclic nucleotide signaling modulates growth cone responses to guidance cues such as Slit (Nguyen-Ba-Charvet et al., 2001) and arborization factors such as Sema3A (Campbell et al., 2001). Further analysis of the signal transduction pathways triggered in arbors in response to Slit1a may illuminate this issue. A second possibility would be that structural differences between the Slit1 and Slit2 proteins lead to different effects on branching, perhaps recruiting different receptor complexes.

We provide here evidence that Slit proteins regulate synaptogenesis. During arbor formation, new branches emerge preferentially from synaptic sites, and synaptogenesis appears to guide arbor growth by the selective stabilization of new branches (Alsina et al., 2001; Javaherian and Cline, 2005; Meyer and Smith, 2006; Ruthazer et al., 2006). Therefore, synaptogenesis and arborization are intertwined so that factors affecting synapse formation may dramatically affect arbor growth. Repeated imaging enabled us to observe individual arbors at different ages during the processes of arborization and synaptogenesis. We found that knockdown of Slit1a protein led to a transient increase in presumptive presynaptic puncta at 76 hpf, but not 86 hpf or 100 hpf, presumably due to the decrease over time in MO effectiveness. However, the arbors in *slit1a* morphants still possessed increased numbers of branch tips, increased areas and complexity until at least 86 hpf, and total arbor lengths and branch tip number were still increased at 100 hpf. Thus, in this case Slit1a knockdown does not seem to have strictly parallel effects on synaptogenesis and arborization. Perhaps a lower level of Slit1a protein is required to regulate synaptogenesis than that required for arborization.

Slit-Robo signaling presumably controls arborization by modulating cytoskeletal dynamics. It will be interesting to elucidate whether arborization and axon pathfinding share the same intracellular signaling pathways. The cytoplasmic domain of Robo receptors contains conserved motifs that are necessary to mediate signal transduction (Patel and Van Vactor, 2002). Members of the enabled/vasodilator-stimulated phosphoprotein (Ena/VASP) family act downstream of Robo receptors (Bashaw et al., 2000) and have been implicated in synaptic plasticity (Kato et al., 1997) as well as RGC branching (Dwivedy et al., 2007). In *Drosophila*, overexpression of Robo in giant fiber neurones can lead to a *bendless*-like phenotype, with premature axon termination (Godenschwege et al., 2002). Godenschwege and coworkers propose that this phenotype is due to a failure to establish synaptic connections with normal target neurones, perhaps because cell-surface Robo must be downregulated to terminate axon growth and begin synaptogenesis. Such a switch does not seem likely in retinotectal arbors, where synaptogenesis proceeds

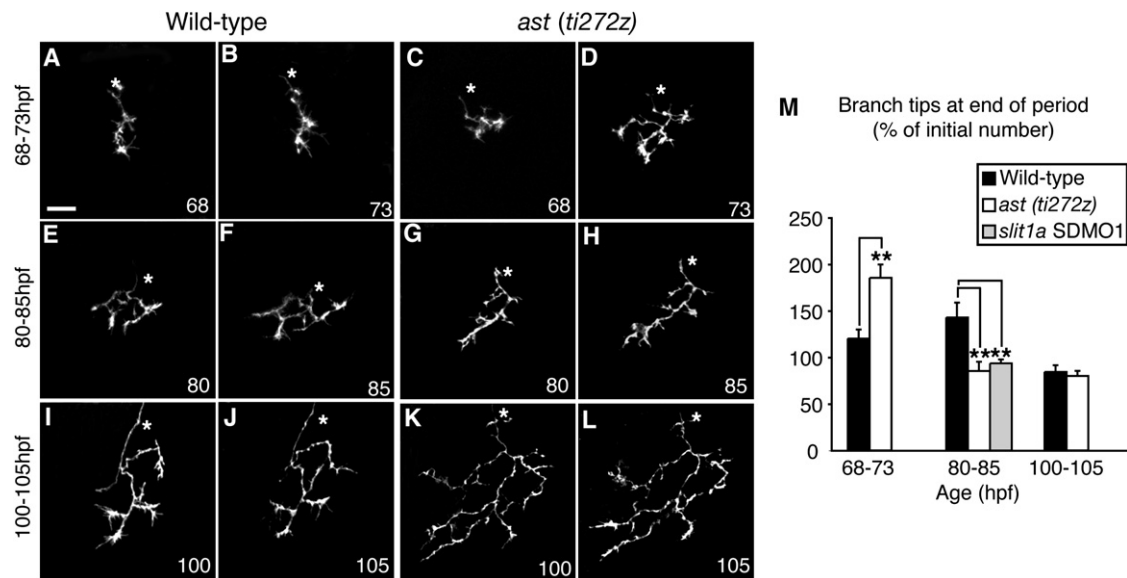


Figure 8. The *astray* Arborization Phenotype Develops Early during Arborization

Confocal images of WT and *ast (ti272z)* RGC arbors, labeled with *brn3c:GAL4, UAS:mGFP*, at the beginning and end of each 5 hr imaging period: 68–73 hpf (A–D), 80–85 hpf (E–H), and 100–105 hpf (I–L); dorsal views, anterior up. *ast* arbors nearly double their branch tip number from 68 to 73 hpf, compared to a much smaller increase in WT (C, D, and M). However, from 80 to 85 hpf, WT arbors increase their branch tip number significantly more than do *ast* and *slit1a* morphants (*slit1a* SDMO1) (E–H and M). During the 100–105 hpf imaging session, WT and *ast* arbors have relatively stable numbers of branch tips (I–M). White * indicates the parent axon. Eight to ten arbors from eight to ten embryos analyzed per genotype. Error bars represent SEM. **p < 0.01. Scale bar, 10 μ m.

simultaneously with arbor growth. We found that loss of Slit-Robo signaling leads to the stabilization of RGC arbor dynamics and premature maturation of RGC arbors. Slit-Robo signaling may normally prevent RGC arborization while the tectum is immature and not ready to receive input. It will be interesting to determine whether Slit-Robo signaling also plays a role in tectal dendrite development, as has been observed for cortical dendrites (Whitford et al., 2002).

To date, BDNF is the only secreted molecule whose role has been tested extensively during RGC arborization and synaptogenesis *in vivo*. BDNF promotes arborization and synaptogenesis of *Xenopus* RGC arbors (Alsina et al., 2001; Cohen-Cory and Fraser, 1995). If BDNF plays a similar role in zebrafish RGCs, the size of retinal arbors may be determined by a balance between arborization promoting and inhibiting factors. Recently, BDNF has been shown to act on cadherins via β -catenin to promote synapse dispersal, leading to increased synapse number (Bamji et al., 2006). Interestingly, *Drosophila* Robo can inhibit N-cadherin β -catenin signaling (Rhee et al., 2002), providing a possible explanation for how the inhibitory effects of Slit-Robo signaling could counteract those of BDNF. We find that Robo2 acts cell-autonomously to inhibit arborization; since a recent study identified a cell-autonomous role for TrkB in RGC arbor maturation (Marshak et al., 2007), it will be interesting to determine whether Robo2 interacts with TrkB in RGC arbors. O'Leary and colleagues have shown the involvement of both EphrinA-EphA signaling

and EphrinB-EphB signaling in controlling the directional branch extension of RGC axons during topographic map formation (Hindges et al., 2002; Yates et al., 2001). Since *slit1a* and *robo2* are expressed uniformly throughout the tectum and in RGCs, it is unlikely that they inhibit arborization and synaptogenesis in a topographically specific manner.

To start to understand the mechanisms by which Slit-Robo signaling inhibits arborization and synaptogenesis in RGCs, we analyzed the genetic interaction between *robo2* and *slit1a*. The similarity of the *ast* and *slit1a* morphant phenotypes, together with the supra-additive phenotype of *ast/+;slit1a* MO arbors, strongly supports the model that *slit1a* inhibits RGC arborization via a *robo2*-dependent mechanism, consistent with previous findings that Robos can act as receptors for Slit proteins (Brose et al., 1999; Kidd et al., 1999; Li et al., 1999). Additionally, however, the enhancement of the *ast* null phenotype by *slit1a* knockdown shows that *slit1a* also inhibits arborization and synaptogenesis via a *robo2*-independent pathway, suggesting the existence of one or more additional receptors. What is its identity? It is presumably not another *robo*, since we did not detect expression of any *robo* genes in RGCs besides *robo2*. Syndecan interacts with Slit and Robo, but apparently as a coreceptor and not via a distinct signaling mechanism (Hohenester et al., 2006). The plexin and neuropilin families of semaphorin receptors (Tamagnone and Comoglio, 2000) are potential candidates, since semaphorins promote or

inhibit arborization (Bagnard et al., 1998; Campbell et al., 2001) and plexinA4 acts downstream of Slit2 to mediate its arborization-promoting effect on zebrafish trigeminal sensory axons (Miyashita et al., 2004). Several members of the neuropilin family are expressed in the zebrafish retina (Liu et al., 2004), although their function remains to be determined.

The complex role of neuronal activity in the retinotectal system has been extensively studied. Activity acts on RGC arbor growth in at least three ways: activity-dependent competition between arbors (Hua et al., 2005); a homeostatic signaling mechanism by which post-synaptic cells promote growth of presynaptic arbors to compensate for reduced synaptic drive (Smear et al., 2007); and Hebbian or spike-timing-dependent plasticity (Dan and Poo, 2004; Hua and Smith, 2004; Ruthazer et al., 2003). In zebrafish, some pathways may not yet be active during the period we studied, since between 3 to 5 dpf, RGC action potentials appear unnecessary for normal arbor development (Gnuegge et al., 2001; Stuermer et al., 1990). The phenotypes that we find with inhibition of Slit1a-Robo2 signaling are distinct from those seen after blocking electrical activity or glutamatergic synaptic transmission. While silencing of electrical activity in individual RGCs leads to smaller arbors than surrounding axons (Hua et al., 2005), inhibiting Robo2 activity in single RGCs leads to more complex arbors. Pharmacological blockade of NMDA receptors leads to increased arbor area and unchanged branch tip number (Schmidt et al., 2000), unlike the larger arbors with *increased* branch tip number that we see in *ast* mutants. Finally, reduced glutamate release in the *blu/vesicular glutamate transporter 2a* mutant leads to an increase in arbor size that is reversed when mutant RGCs are transplanted into wild-type embryos (Smear et al., 2007; M. Smear and H.B., unpublished data), unlike the cell-autonomous effects that we find for loss of Robo2. Further work will be necessary to characterize whether and how Slit signaling may interact with activity-dependent mechanisms.

Through a combination of genetic and in vivo imaging we have shown that Slit-Robo signaling plays roles in inhibiting arborization in vivo in the vertebrate CNS. Our study shows an inhibitory role for Slit-Robo signaling and shows that in this system *slit1a* mediates some of its effects on arborization and synaptogenesis independently of *robo2*. Further work will be necessary to determine the signal transduction mechanisms by which *slit1a* inhibits RGC arborization and synaptogenesis, the nature of the additional receptor(s), and how Slit-Robo signaling interacts with other arborization cues.

EXPERIMENTAL PROCEDURES

Zebrafish Embryos

WT and mutant embryos were obtained by natural matings, raised at 28.5°C, and staged by age and morphology (Kimmel et al., 1995). WT embryos were from Tup-longfin (TL) and Tübingen strains. Because the *ast* alleles *ti272z* and *te284* (Fricke et al., 2001; Karlstrom et al., 1996) are homozygous viable, *ast* embryos were generated by

homozygous incrosses. *ast*+ embryos were generated by crossing *ast* with TL. Experimental protocols were approved by the University of Utah Institutional Animal Care and Use Committee and are in accordance with the NIH Guide for Care and Use of Animals.

DNA Constructs

To generate *brn3c:GAL4VP16,UAS:mGFP*, an EcoRI fragment containing 14xUAS-e1b (from pBUASe1b, generated by R. Köster) was inserted into the *pbrn3c:mGFP* vector (Xiao et al., 2005), and a PCR product for GAL4VP16-SV40 polyA was inserted into the StuI site after the *brn3c* promoter. To generate *brn3c:GAL4VP16*, UAS and mGFP were removed using Apal and PstI, followed by end-blunting and self-ligation.

To generate *isl3:GAL4VP16*, a 17.6 kb genomic fragment containing the *isl3* (*isl3*) enhancer-promoter (A.J. Pittman and C.-B.C., unpublished data) was used to generate a Gateway (Invitrogen) destination vector. GAL4VP16 (a gift from R. Köster) was PCR amplified to generate the pME-Gal4VP16 Gateway entry clone and placed downstream of the *isl3* fragment by Gateway recombination.

To generate *UAS:YFP-rab3*, cDNA sequence for a zebrafish homolog of Rab3 was amplified from IMAGE clone 4966168 (GenBank accession BI428994) using oligonucleotides 5'-AAAAGGTACCA GATGGCTGTACACAAGACAAC-3' and 5'-TTTCCGCGCGTACAG CAGCTGCAGTCTGACGGC-3', digested with Acc65I/EagI and inserted into BsrGI/NotI-digested pUAS-mcs-YFP, 3' to the YFP. pUAS-mcs-YFP (M.L.N., unpublished data) is a derivative of pUAS-mYFP (Schroeter et al., 2006) in which a master cloning site and YFP have replaced the mYFP sequence (M.L.N., unpublished data). The Rab3 coding sequence was confirmed by sequencing. *UAS:YFP-rab3* sequences were moved into the Tol2 vector pBH (A.T. and M.L.N., unpublished data) to create pBH-UAS:YFP-rab3 and were used to create the transgenic line *Tg(pBH UAS:YFP-rab3)^{nm1}* using standard methods (Kawakami, 2004). Sequences are available at <http://thalamus.wustl.edu/nonetlab/ResourcesF>.

Gateway entry clones pME-Robo2 and pME-Robo2 dC(no stop) were generated by PCR amplification and BP recombination, then used with constructs from the Tol2kit system (K. Kwan, C.-B.C., et al., unpublished data) to generate *UAS:Robo2* expression clones by Gateway LR recombination. pME-Robo2 and pME-mCherry were combined with p5E-UAS, p3E-EGFP-CAAX-pA, and pDestTol2CG2 to yield pDestTol2CG2;UAS:Robo2-IRES-EGFP-CAAX and pDest-Tol2CG2;UAS:mCherry-IRES-EGFP-CAAX, respectively. pME-Robo2 dC(no stop) was combined with p5E-UAS, p3E-EGFP-pA, and pDest R4-R3 (Invitrogen) to yield pDest R4-R3;UAS:Robo2ΔC-EGFP. Details of cloning are available upon request.

Morpholino Injections

A "standard control" MO (control MO; 5'-CCTCTTACCTCAGTTA CAATTTATA-3') was compared to two *slit1a* MOs (Gene Tools): a translation-blocking MO1 (*slit1a* trans MO1; 5'-GACAACATCCTCC TCTCGCAGGCAT-3') (Barresi et al., 2005) and a splice-blocking MO (*slit1a* SDMO1; 5'-GAAATAAACTCACAGCCTCTCGGTG-3') whose efficacy has been confirmed by RT-PCR (L.D. Hutson, D.S.C., and C.-B.C., unpublished data). MOs were diluted to 2 ng/μl (combined with DNA constructs for labeling) and injected at final volume of 1 nl (bolus calibrated by eyepiece micrometer) into one cell at the one to four-cell stage. High doses of *slit1a* MO can yield morphological phenotypes; these doses were carefully chosen to yield normal overall morphology, and so likely remove *slit1a* function only partially.

RGC Arbor and Presynaptic Labeling

Single RGC axons were labeled by mosaic expression of a *brn3c:GAL4VP16, UAS:mGFP* construct after microinjection of ~1 nl of 35 ng/μl DNA into one cell of one- to four-cell embryos (Hutson et al., 2004). Presumptive presynaptic sites were labeled by coinjection of 25 ng/μl *brn3c:GAL4VP16* or *isl3:GAL4VP16* and 25 ng/μl *UAS:YFP-rab3*. Embryos were screened for single labeled arbors on the tectum

at 76 hpf using a 60×/1.2NA water-immersion objective. For consistency, arbors analyzed were always from caudomedial tectum (Schmidt et al., 2000; Tokuoka et al., 2002).

Imaging and Quantitative Analysis of Retinal Arbors

Embryos were mounted in 1.5% NuSieve low melting point (LMP) agarose in 35 mm glass-bottomed Petri dishes. Retinal arbors and presynaptic sites were imaged using an Olympus Fluoview 300 laser-scanning confocal microscope equipped with a 60×/1.2NA water-immersion objective. Membrane-targeted mGFP5 and YFP were excited at 488 nm and detected with a 510 nm long-pass emission filter. 2.0 μm optical sections were captured at 512 × 512 pixels, zoom 3, 0.15 pixels/μm. Care was taken to avoid pixel saturation.

Images were analyzed as maximum-intensity z projections of unmanipulated images in ImageJ software (W.S. Rasband, National Institutes of Health, <http://rsb.info.nih.gov/ij/>, 1997–2003). Branch tips were counted when ≥5.0 μm in length. Total branch lengths were measured using the segmented line tool. Arbor areas were determined by drawing a convex polygon connecting the branch tips using the polygon tool. Arbor order was defined as the mean number of branch points between a terminal branch and the parent axon (Schmidt et al., 2000; Tokuoka et al., 2002) (Figure S2). Presynaptic Rab3-YFP⁺ sites were counted by thresholding (Tokuoka et al., 2002; Figure 5). A punctum was defined as an area of ≥2 pixels whose intensity was ≥5× that of a nonpunctate region of the same arbor.

Time-Lapse Imaging of Retinal Arbors

Time-lapse imaging of membrane-targeted (mGFP) labeled WT, *ast*, and *slit1a* morphant retinal arbors was performed on an Olympus FV1000 laser-scanning confocal microscope or an upright Olympus FVX confocal custom-modified for two-photon imaging (Majewska et al., 2000; Nikolenko et al., 2003) (modified by B. Mangum). Embryos were anesthetized in 0.004% tricaine, then mounted in 1.5% LMP agarose in coverslip-bottomed petri dishes (FV1000) or on a microscope slide, with a surrounding wax reservoir formed from dental wax (two-photon). FV1000 imaging used 488 nm excitation and a 60×/1.2 W objective; two-photon imaging used a Ti:Sapphire laser tuned to 880 nm (Coherent, Santa Clara, CA) and a 60×/0.9 W objective. Z stacks of 10 to 30 slices, 2.0 μm spacing were captured every 15 min for 5 hr during the periods 68–73, 80–85, and 100–105 hpf. Afterward, embryo viability was assessed by blood flow and heartbeat. The ImageJ grouped z projector plugin was used to save maximum-intensity projections from each time point as 8 bit TIFF files, which were analyzed in Object Image (<http://simon.bio.uva.nl/object-image.html>) using morphometry macros written by Dr. E. Ruthazer (<http://clinelab.cshl.edu/methods.html>).

In Situ Hybridization

Whole-mount in situ hybridization was performed on WT, *ast*, and *slit1a* morphant embryos as described (Lee et al., 2001). Digoxigenin-labeled antisense mRNA probes were synthesized for *robo1*, 2, 3, and 4 (Challa et al., 2001; Lee et al., 2001; Park et al., 2003) and *slit1a*, 1b, 2, and 3 (Hutson et al., 2003; Yeo et al., 2001), *mbx-s* (Kawahara et al., 2002), *fgf8* (Reifers et al., 1998), and *tbx5* (Tamura et al., 1999). Embryos were mounted in 100% glycerol, coverslipped, and photographed on an Olympus BXWS1W1 compound microscope using a Microfire CCD camera and Picture Frame software (Olympus). For sections, whole-mount in situ hybridized embryos were embedded in 20% gelatin in PBS, fixed in 4% PFA, sectioned at 50 μm on a vibratome (Leica), coverslipped in 80% glycerol, and photographed.

Statistical Analysis

Statistical analyses were performed using InStat3 (GraphPad) and Statview (Abacus Concepts Inc). Nonparametric statistical analyses were performed using the Mann-Whitney U test, allowing for whether standard deviations of the conditions being compared were signifi-

cantly different. Data are presented as mean values plus or minus SEM.

Supplemental Data

The Supplemental Data for this article can be found online at <http://www.neuron.org/cgi/content/full/55/2/231/DC1>.

ACKNOWLEDGMENTS

We thank Lara Hutson for the *slit1a* morpholinos, Andrew Pittman for the *isf3* promoter, Benjamin Mangum for the two-photon microscope conversion, Edward Ruthazer for advice for using his Object Image Morphometry macros, the Dorsky lab for use of their microscope and camera, Hitoshi Okamoto and Deborah Yelon for in situ probes, Susan Chapman for advice with sectioning, Reinhard Köster for plasmids, and Sherry Scott for critical reading of the manuscript. We are very grateful to Hitoshi Okamoto in whose laboratory some of the experiments were carried out. Time-lapse imaging was performed at the University of Utah School of Medicine Cell Imaging Facility and at the RIKEN Brain Science Institute. This work was supported by a European Molecular Biology Program Long-Term Fellowship and a Japan Society for the Promotion of Science post-doctoral fellowship (D.S.C.), a Neuroscience training grant postdoctoral fellowship (T.X.), grants from the NIH/NEI (EY12406, EY13855) and March of Dimes (H.B.), grants from the McDonnell Center for Cellular Neuroscience and the National Institutes of Health (M.L.N.), and a grant from the NIH/NEI (EY12873, C.-B.C.).

Received: October 9, 2006

Revised: May 30, 2007

Accepted: June 28, 2007

Published: July 18, 2007

REFERENCES

- Alsina, B., Vu, T., and Cohen-Cory, S. (2001). Visualizing synapse formation in arborizing optic axons in vivo: dynamics and modulation by BDNF. *Nat. Neurosci.* 4, 1093–1101.
- Bagnard, D., Lohrum, M., Uziel, D., Puschel, A.W., and Bolz, J. (1998). Semaphorins act as attractive and repulsive guidance signals during the development of cortical projections. *Development* 125, 5043–5053.
- Bamji, S.X., Rico, B., Kimes, N., and Reichardt, L.F. (2006). BDNF mobilizes synaptic vesicles and enhances synapse formation by disrupting cadherin-β-catenin interactions. *J. Cell Biol.* 174, 289–299.
- Barresi, M.J., Hutson, L.D., Chien, C.B., and Karlstrom, R.O. (2005). Hedgehog regulated Slit expression determines commissure and glial cell position in the zebrafish forebrain. *Development* 132, 3643–3656.
- Bashaw, G.J., Kidd, T., Murray, D., Pawson, T., and Goodman, C.S. (2000). Repulsive axon guidance: Abelson and Enabled play opposing roles downstream of the roundabout receptor. *Cell* 101, 703–715.
- Brose, K., Bland, K.S., Wang, K.H., Arnott, D., Henzel, W., Goodman, C.S., Tessier-Lavigne, M., and Kidd, T. (1999). Slit proteins bind Robo receptors and have an evolutionarily conserved role in repulsive axon guidance. *Cell* 96, 795–806.
- Campbell, D.S., Regan, A.G., Lopez, J.S., Tannahill, D., Harris, W.A., and Holt, C.E. (2001). Semaphorin 3A elicits stage-dependent collapse, turning, and branching in *Xenopus* retinal growth cones. *J. Neurosci.* 21, 8538–8547.
- Challa, A.K., Beattie, C.E., and Seeger, M.A. (2001). Identification and characterization of roundabout orthologs in zebrafish. *Mech. Dev.* 101, 249–253.

- Cohen-Cory, S., and Fraser, S.E. (1995). Effects of brain-derived neurotrophic factor on optic axon branching and remodelling in vivo. *Nature* 378, 192–196.
- Dan, Y., and Poo, M.M. (2004). Spike timing-dependent plasticity of neural circuits. *Neuron* 44, 23–30.
- Dwivedy, A., Gertler, F.B., Miller, J., Holt, C.E., and Lebrand, C. (2007). Ena/VASP function in retinal axons is required for terminal arborization but not pathway navigation. *Development* 134, 2137–2146.
- Easter, S.S., Jr., and Nicola, G.N. (1996). The development of vision in the zebrafish (*Danio rerio*). *Dev. Biol.* 180, 646–663.
- Fricke, C., Lee, J.S., Geiger-Rudolph, S., Bonhoeffer, F., and Chien, C.B. (2001). *astray*, a zebrafish roundabout homolog required for retinal axon guidance. *Science* 292, 507–510.
- Gnuegge, L., Schmid, S., and Neuhaus, S.C. (2001). Analysis of the activity-deprived zebrafish mutant *macho* reveals an essential requirement of neuronal activity for the development of a fine-grained visuotopic map. *J. Neurosci.* 21, 3542–3548.
- Godenschwege, T.A., Simpson, J.H., Shan, X., Bashaw, G.J., Goodman, C.S., and Murphey, R.K. (2002). Ectopic expression in the giant fiber system of *Drosophila* reveals distinct roles for roundabout (*Robo*), *Robo2*, and *Robo3* in dendritic guidance and synaptic connectivity. *J. Neurosci.* 22, 3117–3129.
- Hindges, R., McLaughlin, T., Genoud, N., Henkemeyer, M., and O'Leary, D.D. (2002). EphB forward signaling controls directional branch extension and arborization required for dorsal-ventral retinotopic mapping. *Neuron* 35, 475–487.
- Hohenester, E., Hussain, S., and Howitt, J.A. (2006). Interaction of the guidance molecule Slit with cellular receptors. *Biochem. Soc. Trans.* 34, 418–421.
- Hua, J.Y., and Smith, S.J. (2004). Neural activity and the dynamics of central nervous system development. *Nat. Neurosci.* 7, 327–332.
- Hua, J.Y., Smear, M.C., Baier, H., and Smith, S.J. (2005). Regulation of axon growth in vivo by activity-based competition. *Nature* 434, 1022–1026.
- Hutson, L.D., and Chien, C.B. (2002). Pathfinding and error correction by retinal axons: the role of *astray/robo2*. *Neuron* 33, 205–217.
- Hutson, L.D., Jurynek, M.J., Yeo, S.Y., Okamoto, H., and Chien, C.B. (2003). Two divergent slit1 genes in zebrafish. *Dev. Dyn.* 228, 358–369.
- Hutson, L.D., Campbell, D.S., and Chien, C.B. (2004). Analyzing axon guidance in the zebrafish retinotectal system. *Methods Cell Biol.* 76, 13–35.
- Javaherian, A., and Cline, H.T. (2005). Coordinated motor neuron axon growth and neuromuscular synaptogenesis are promoted by CPG15 in vivo. *Neuron* 45, 505–512.
- Jin, Y. (2002). Synaptogenesis: insights from worm and fly. *Curr. Opin. Neurobiol.* 12, 71–79.
- Karlstrom, R.O., Trowe, T., Klostermann, S., Baier, H., Brand, M., Crawford, A.D., Grunewald, B., Haffter, P., Hoffmann, H., Meyer, S.U., et al. (1996). Zebrafish mutations affecting retinotectal axon pathfinding. *Development* 123, 427–438.
- Kato, A., Ozawa, F., Saitoh, Y., Hirai, K., and Inokuchi, K. (1997). *vesl*, a gene encoding VASP/Ena family related protein, is upregulated during seizure, long-term potentiation and synaptogenesis. *FEBS Lett.* 412, 183–189.
- Kawahara, A., Chien, C.B., and Dawid, I.B. (2002). The homeobox gene *mbx* is involved in eye and tectum development. *Dev. Biol.* 248, 107–117.
- Kawakami, K. (2004). Transgenesis and gene trap methods in zebrafish by using the Tol2 transposable element. *Methods Cell Biol.* 77, 201–222.
- Kidd, T., Bland, K.S., and Goodman, C.S. (1999). Slit is the midline repellent for the robo receptor in *Drosophila*. *Cell* 96, 785–794.
- Kimmel, C.B., Ballard, W.W., Kimmel, S.R., Ullmann, B., and Schilling, T.F. (1995). Stages of embryonic development of the zebrafish. *Dev. Dyn.* 203, 253–310.
- Köster, R.W., and Fraser, S.E. (2001). Tracing transgene expression in living zebrafish embryos. *Dev. Biol.* 233, 329–346.
- Lee, J.S., Ray, R., and Chien, C.B. (2001). Cloning and expression of three zebrafish roundabout homologs suggest roles in axon guidance and cell migration. *Dev. Dyn.* 221, 216–230.
- Lee, J.S., von der Hardt, S., Rusch, M.A., Stringer, S.E., Stickney, H.L., Talbot, W.S., Geisler, R., Nusslein-Volhard, C., Selleck, S.B., Chien, C.B., and Roehl, H. (2004). Axon sorting in the optic tract requires HSPG synthesis by *ext2* (*dackel*) and *ext3* (*boxer*). *Neuron* 44, 947–960.
- Li, H.S., Chen, J.H., Wu, W., Fagaly, T., Zhou, L., Yuan, W., Dupuis, S., Jiang, Z.H., Nash, W., Gick, C., et al. (1999). Vertebrate slit, a secreted ligand for the transmembrane protein roundabout, is a repellent for olfactory bulb axons. *Cell* 96, 807–818.
- Liu, Y., Berndt, J., Su, F., Tawarayama, H., Shoji, W., Kuwada, J.Y., and Halloran, M.C. (2004). Semaphorin3D guides retinal axons along the dorsoventral axis of the tectum. *J. Neurosci.* 24, 310–318.
- Majewska, A., Yiu, G., and Yuste, R. (2000). A custom-made two-photon microscope and deconvolution system. *Pflugers Arch.* 441, 398–408.
- Marshak, S., Nikolakopoulou, A.M., Dirks, R., Martens, G.J., and Cohen-Cory, S. (2007). Cell-autonomous TrkB signaling in presynaptic retinal ganglion cells mediates axon arbor growth and synapse maturation during the establishment of retinotectal synaptic connectivity. *J. Neurosci.* 27, 2444–2456.
- Meyer, M.P., and Smith, S.J. (2006). Evidence from in vivo imaging that synaptogenesis guides the growth and branching of axonal arbors by two distinct mechanisms. *J. Neurosci.* 26, 3604–3614.
- Miyashita, T., Yeo, S.Y., Hirate, Y., Segawa, H., Wada, H., Little, M.H., Yamada, T., Takahashi, N., and Okamoto, H. (2004). PlexinA4 is necessary as a downstream target of *Islet2* to mediate Slit signaling for promotion of sensory axon branching. *Development* 131, 3705–3715.
- Nguyen-Ba-Charvet, K.T., Brose, K., Marillat, V., Sotelo, C., Tessier-Lavigne, M., and Chedotal, A. (2001). Sensory axon response to substrate-bound Slit2 is modulated by laminin and cyclic GMP. *Mol. Cell. Neurosci.* 17, 1048–1058.
- Niell, C.M., Meyer, M.P., and Smith, S.J. (2004). In vivo imaging of synapse formation on a growing dendritic arbor. *Nat. Neurosci.* 7, 254–260.
- Nikolenko, V., Nemet, B., and Yuste, R. (2003). A two-photon and second-harmonic microscope. *Methods* 30, 3–15.
- Park, K.W., Morrison, C.M., Sorensen, L.K., Jones, C.A., Rao, Y., Chien, C.B., Wu, J.Y., Urness, L.D., and Li, D.Y. (2003). *Robo4* is a vascular-specific receptor that inhibits endothelial migration. *Dev. Biol.* 261, 251–267.
- Patel, B.N., and Van Vactor, D.L. (2002). Axon guidance: the cytoplasmic tail. *Curr. Opin. Cell Biol.* 14, 221–229.
- Plump, A.S., Erskine, L., Sabatier, C., Brose, K., Epstein, C.J., Goodman, C.S., Mason, C.A., and Tessier-Lavigne, M. (2002). Slit1 and Slit2 cooperate to prevent premature midline crossing of retinal axons in the mouse visual system. *Neuron* 33, 219–232.
- Reifers, F., Bohlh, H., Walsh, E.C., Crossley, P.H., Stainier, D.Y., and Brand, M. (1998). *Fgf8* is mutated in zebrafish *acerebellar* (*ace*) mutants and is required for maintenance of midbrain-hindbrain boundary development and somitogenesis. *Development* 125, 2381–2395.
- Rhee, J., Mahfooz, N.S., Arregui, C., Lilien, J., Balsamo, J., and VanBerkum, M.F. (2002). Activation of the repulsive receptor Roundabout inhibits N-cadherin-mediated cell adhesion. *Nat. Cell Biol.* 4, 798–805.

- Ruthazer, E.S., Li, J., and Cline, H.T. (2006). Stabilization of axon branch dynamics by synaptic maturation. *J. Neurosci.* *26*, 3594–3603.
- Ruthazer, E.S., Akerman, C.J., and Cline, H.T. (2003). Control of axon branch dynamics by correlated activity in vivo. *Science* *301*, 66–70.
- Schmidt, J.T., Buzzard, M., Borress, R., and Dhillon, S. (2000). MK801 increases retinotectal arbor size in developing zebrafish without affecting kinetics of branch elimination and addition. *J. Neurobiol.* *42*, 303–314.
- Schroeter, E.H., Wong, R.O., and Gregg, R.G. (2006). In vivo development of retinal ON-bipolar cell axonal terminals visualized in *nyx:MYFP* transgenic zebrafish. *Vis. Neurosci.* *23*, 833–843.
- Smear, M.C., Tao, H.W., Staub, W., Orger, M.B., Gosse, N.J., Liu, Y., Takahashi, K., Poo, M.M., and Baier, H. (2007). Vesicular glutamate transport at a central synapse limits the acuity of visual perception in zebrafish. *Neuron* *53*, 65–77.
- Stein, E., and Tessier-Lavigne, M. (2001). Hierarchical organization of guidance receptors: silencing of netrin attraction by slit through a Robo/DCC receptor complex. *Science* *291*, 1928–1938.
- Stuermer, C.A. (1988). Retinotopic organization of the developing retinotectal projection in the zebrafish embryo. *J. Neurosci.* *8*, 4513–4530.
- Stuermer, C.A., Rohrer, B., and Munz, H. (1990). Development of the retinotectal projection in zebrafish embryos under TTX-induced neural-impulse blockade. *J. Neurosci.* *10*, 3615–3626.
- Sudhof, T.C. (2004). The synaptic vesicle cycle. *Annu. Rev. Neurosci.* *27*, 509–547.
- Tamagnone, L., and Comoglio, P.M. (2000). Signalling by semaphorin receptors: cell guidance and beyond. *Trends Cell Biol.* *10*, 377–383.
- Tamura, K., Yonei-Tamura, S., and Belmonte, J.C. (1999). Differential expression of *Tbx4* and *Tbx5* in Zebrafish fin buds. *Mech. Dev.* *87*, 181–184.
- Tokuoka, H., Yoshida, T., Matsuda, N., and Mishina, M. (2002). Regulation by glycogen synthase kinase-3 β of the arborization field and maturation of retinotectal projection in zebrafish. *J. Neurosci.* *22*, 10324–10332.
- Waites, C.L., Craig, A.M., and Garner, C.C. (2005). Mechanisms of vertebrate synaptogenesis. *Annu. Rev. Neurosci.* *28*, 251–274.
- Wang, K.H., Brose, K., Arnott, D., Kidd, T., Goodman, C.S., Henzel, W., and Tessier-Lavigne, M. (1999). Biochemical purification of a mammalian slit protein as a positive regulator of sensory axon elongation and branching. *Cell* *96*, 771–784.
- Whitford, K.L., Marillat, V., Stein, E., Goodman, C.S., Tessier-Lavigne, M., Chedotal, A., and Ghosh, A. (2002). Regulation of cortical dendrite development by Slit-Robo interactions. *Neuron* *33*, 47–61.
- Wong, K., Park, H.T., Wu, J.Y., and Rao, Y. (2002). Slit proteins: molecular guidance cues for cells ranging from neurons to leukocytes. *Curr. Opin. Genet. Dev.* *12*, 583–591.
- Xiao, T., Roeser, T., Staub, W., and Baier, H. (2005). A GFP-based genetic screen reveals mutations that disrupt the architecture of the zebrafish retinotectal projection. *Development* *132*, 2955–2967.
- Yates, P.A., Roskies, A.L., McLaughlin, T., and O'Leary, D.D. (2001). Topographic-specific axon branching controlled by ephrin-As is the critical event in retinotectal map development. *J. Neurosci.* *21*, 8548–8563.
- Yeo, S.Y., Little, M.H., Yamada, T., Miyashita, T., Halloran, M.C., Kuwada, J.Y., Huh, T.L., and Okamoto, H. (2001). Overexpression of a slit homologue impairs convergent extension of the mesoderm and causes cyclopia in embryonic zebrafish. *Dev. Biol.* *230*, 1–17.
- Yeo, S.Y., Miyashita, T., Fricke, C., Little, M.H., Yamada, T., Kuwada, J.Y., Huh, T.L., Chien, C.B., and Okamoto, H. (2004). Involvement of *Islet-2* in the Slit signaling for axonal branching and defasciculation of the sensory neurons in embryonic zebrafish. *Mech. Dev.* *121*, 315–324.